geoconvention
Virtual Event
September 13 - 15
2021

# Moment-tensor inversion of hydraulic-fracturing induced events in a Montney reservoir, northeastern BC

*Hanh Bui and Mirko van der Baan*
*Dept. of Physics, University of Alberta*

## Summary

Source mechanisms help understand the fracturing behavior and the evolving stress field in microseismic monitoring. This study presents how to retrieve the source mechanisms of hydraulic-fracturing induced events using a source mechanism screening test based on the S/P amplitude ratio and a full inversion. We estimate moment tensors of over 1000 microseismic events in a Montney reservoir, northeastern British Colombia (BC). The inversion results are compared with the screening test results, and two methods show good agreement. We have tensile and shear faultings in the study area, with tensile mechanisms highly likely being dominant in stages towards the heel of the well.

## Theory / Method

### *A rough estimate of moment tensors from amplitude ratios*

The S/P amplitude ratios can provide useful information about the source mechanisms of microseismic events (Eaton et al., 2014; Walter and Brune, 1993; Pearson, 1981). Pearson (1981) examined the S/P amplitude ratio for shear and tensile faulting and concluded that the ratios for tensile fractures are smaller than 4 while the ratios for shear events can be considerably higher. Walter and Brune (1993) compared the far-field source spectra for tensile and shear-slip events and showed that low S/P spectral amplitude ratios often indicate tensile ruptures. Eaton et al. (2014) investigated the P- and S-wave radiation patterns and suggested that microseismic events with S/P amplitude ratios of less than 5 are most likely tensile events and larger than 5 could be shear events. Therefore, we could use the S/P amplitude ratios estimated from the recordings to have a quick screening of source mechanisms (tensile or shear) without knowing any prior knowledge of the sources.

### *Moment-tensor inversion using amplitude-based methods*

The moment-tensor inversion algorithm calculates Green's functions using the equations for particle motion generated by the P- and S-wave radiations from a point source in a homogeneous elastic medium (Aki and Richards, 2002). The P- and S-wave amplitudes recorded on a given receiver at position x and time t are given as

$$a_i^P(x,t) = \frac{1}{4\pi r\rho\alpha^3}\{\gamma_i\gamma_j\gamma_k M_{jk}\}, \quad (1)$$

$$a_i^S(x,t) = \frac{1}{4\pi r\rho\beta^3}\{(\delta_{ij} - \gamma_i\gamma_j)\gamma_k M_{jk}\}, \quad (2)$$

where $i$ is the component, $r$ is the source-receiver distance, $\rho$ is the density, $\alpha$ is the P-wave velocity, $\beta$ is the S-wave velocity, $\gamma_i$ is the direction cosine from the source to the receiver, $M$ is the moment tensor, and $\delta_{ij}$ is the Kronecker delta. For a non-homogeneous velocity model (e.g., 1D layered velocity model), we use the 1D ray bending algorithm to calculate the average P-wave

velocity and S-wave velocity along the ray path. The amplitudes in equations (1) and (2) can be re-written in a matrix form as

$$\begin{bmatrix} d_1 \\ d_2 \\ \vdots \\ d_n \end{bmatrix} = \begin{bmatrix} G_{11} & G_{12} & G_{13} & G_{14} & G_{15} & G_{16} \\ \vdots & \vdots & \vdots & \vdots & \vdots & \vdots \\ G_{n1} & G_{n2} & G_{n3} & G_{n4} & G_{n5} & G_{n6} \end{bmatrix} \begin{bmatrix} m_1 \\ m_2 \\ \vdots \\ m_6 \end{bmatrix}, \quad (3)$$

where $d_i$ are the observed ground displacement amplitudes at different arrival times at receiver $i$ ($i$ = 1: $n$, $n$ is the number of receivers); $G$ is an nx6 matrix containing the Green's functions calculated using an appropriate velocity model and $m_i$ are the 6 elements of the moment tensor. We have an overdetermined system of linear equations with n equations and only 6 unknowns, which is solved by a least-squares solution (Menke, 2018)

$$m = (G^T G)^{-1} G^T d. \quad (4)$$

The moment tensors obtained from equation (4) can be visualized using Hudson's source-type plot (Hudson et al., 1989).

## Results

We estimate the moment tensors of over 1000 microseismic events (with SNR > 6) detected from 20 hydraulic fracturing (HF) treatment stages in well 2 in a Montney reservoir, northeastern BC (Bui and van der Baan, 2020). Figure 1 shows the locations of the treatment wells, the monitoring arrays (a vertical array with 30 sensors and a horizontal array with 16 sensors), and the events.

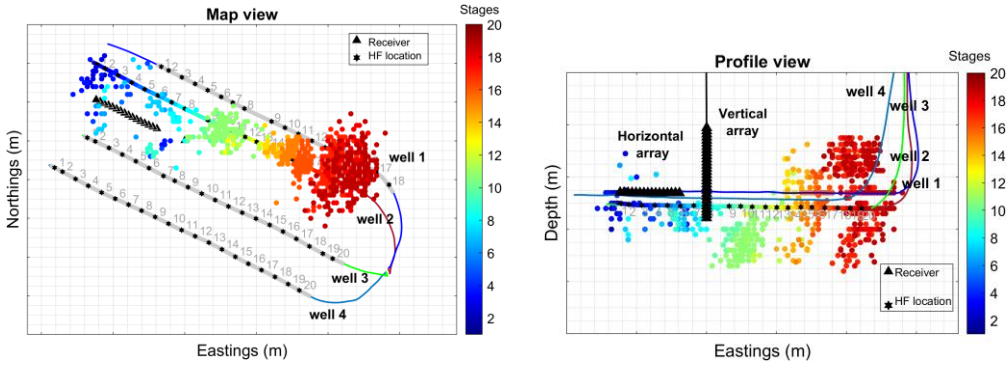


**Figure 1** - Map view and profile view of the events.

### *A first estimate of moment tensors from amplitude ratios*

We select P- and S-wave segments that contain most of the wave energy and compute the root-mean-square (RMS) of the maximum absolute amplitudes of three data components. Then, we calculate the ratios between the peak S-wave amplitude and the peak P-wave amplitude. The final S/P amplitude ratio for each event is the median value between different receivers. We observe a shear-wave splitting in the data, with the shear waves arriving at different times in 3 components. Thus, we carefully select the P- and S-wave windows to ensure the windows be long enough to contain the peak amplitude. The window starts are determined based on the P- and S-wave time picks. We use a fixed S-window length of 0.125 s for all computations and a dynamic P-window length depending on the S-P arrival time differences. We use a P-window of length 0.05 s for the events with S-P arrival time differences larger than 0.05 s. For the events having P- and S-phases close to each other (those events are often near the monitoring wells), the P-window starts from P picks and ends 0.0005 s before the S picks to ensure only P-wave

amplitudes are selected. After obtaining the S/P amplitude ratios, we classify the results into tensile events if the ratio is smaller than 5, and if the ratio is larger than 5, we consider the events as shear events. This permits the first classification into the number of shear and tensile events per stage, which can then be compared with the subsequent full inversion results.

In the first instance, we treat the horizontal and vertical monitoring wells separately, obtaining possibly two contradicting solutions. This is done to simplify the computations but also to get some ideas about uncertainty. Figure 2 shows the results calculated from the vertical-array data and from the horizontal-array data. The results show a similar characteristic, with tensile mechanisms being prominent in well 2, particularly in stages towards the heel of the well (e.g., stages 18, 19, 20). Hundreds of events are likely to have tensile faulting in the stages from 18 to 20. In stages having a few events (e.g., 1, 2, 7, 8, 14-16), we observe a similar feature with more tensile than shear failure.

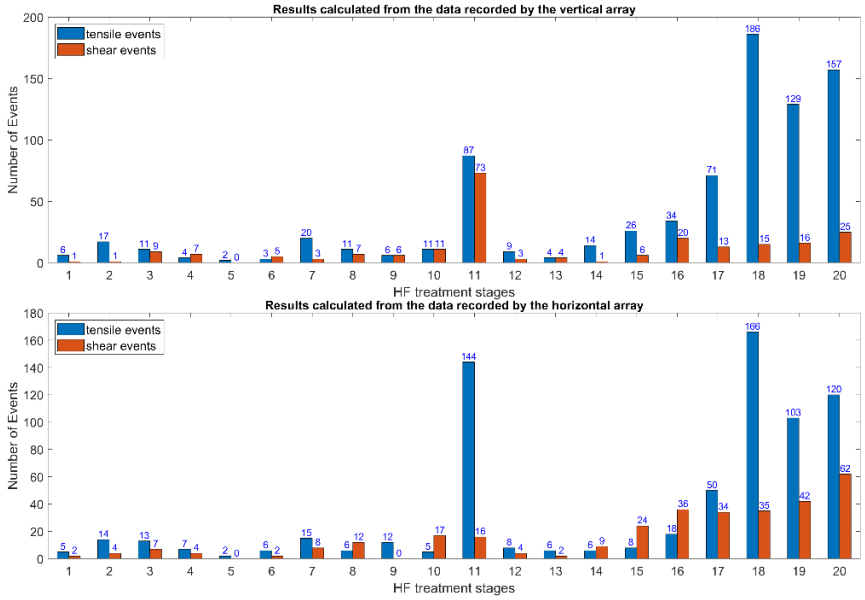


**Figure 2** - S/P amplitude ratios result from the vertical-array and horizontal-array data. Tensile events are indicated by blue color; shear events are indicated by orange color. The numbers in the figures show the number of tensile/shear events in each stage.

### *Moment-tensor inversion using amplitude-based methods*

The inversion algorithm calculates the moment tensors using the P- and S-wave amplitudes from windows determined based on P- and S-wave time picks. We use a fixed S-wave window and a dynamic P-wave window defined as above. The inversion uses the first peak (maximum value) or trough (minimum value) in the P- and S-wave windows. We select the amplitude data from 44 receivers in two arrays as two sensors (2 and 32) did not record the data properly in some stages. The ground displacement vector, d, has the size of 44 x 1 elements. The Green's function G (with a size of 44x6) is calculated using a 1D raytracing program. The moment tensor (m size of 6x1) is then obtained through a least-squares solution using equation (4).

Figure 3 shows Hudson's source-type plots for visualizing the preliminary inversion results of microseismic events in well 2. We plot the results of every five stages (stages 1-5, 6-10, 11-15, and 16-20). Stages 1-5 have 3 clusters of events in the center, top-left, and bottom-right of Hudson's plots. We have both tensile (opening/closing cracks) and shear faultings in these stages. The plot shows that the tensile mechanisms are prominent with more events (indicated

by blue points) adjacent to the tensile opening/closing edges. The inversion results are in good agreement with the screening test from the S/P amplitude ratios shown in Figure 2. Stages 6-10 and 11-15 also show similar characteristics as stages 1-5, which have tensile and shear faultings with tensile mechanisms dominating; although we observe the cluster of solutions is quite spread out; some events are not in the DC and tensile cracks (TC) regions. Overall, the inversion results are in line with the initial results obtained from the S/P amplitude ratios shown in Figure 2. For stages 15-20, the solutions are spread out in the Hudson plot and do not show similar features as stages 1-15. It is possible that the spread in solutions for stages 15-20 is indicative of the presence of an anisotropic velocity field, which is ignored in our inversion.

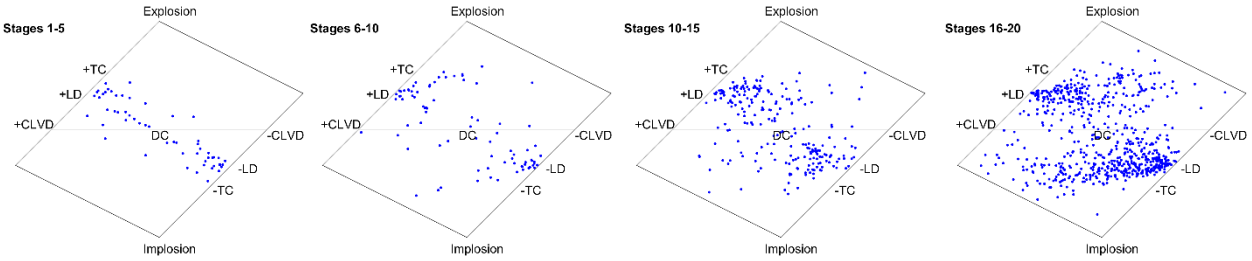


**Figure 3** - Hudson's source-type plots for visualizing the moment-tensor inversion results of microseismic events in well 2.

## Conclusions

This study uses the S/P amplitude ratios as a screening test before performing the full inversion. Although it is not an absolute test, we observe the overall trend of tensile mechanisms being dominant. The test results can support the inversion results. The test shows that we have tensile and shear faultings, with tensile events being highly likely prominent in well 2. The preliminary inversion results on the induced microseismicity, especially in stages 1-15, have a good agreement with the screening test results. We have both types of faultings, but tensile failure dominates towards the well's heel.

## Acknowledgements

The authors would like to thank the sponsors of the Microseismic Industry Consortium for financial support and an anonymous company for permission to use and show the dataset. The authors would like to thank Dr. Thomas Eyre for providing the moment-tensor inversion codes.

### References

Aki, K., and P. G. Richards, 2002, Quantitative seismology, 2nd ed.: University Science Books, 700.
Bui, H., and M. van der Baan, 2020, Event detection using a fast matched filter algorithm - An efficient way to deal with big microseismic datasets: 90th Annual International Meeting, SEG, Expanded Abstracts, 1325-1329.
Eaton, D. W., M. van der Baan, B. Birkelo, and J.-B. Tary, 2014, Scaling relations and spectral characteristics of tensile microseisms: Evidence for opening/closing cracks during hydraulic fracturing: Geophysical Journal International, **196**, 1844-1857.
Hudson, J. A., R. G. Pearce, and R. M. Rogers, 1989, Source type plot for inversion of the moment tensor: Journal of Geophysical Research, **94**, 765-774.
Menke, W., 2018, Geophysical data analysis: Discrete inverse theory, Academic Press.
Pearson, C., 1981, The relationship between microseismicity and high pore pressures during hydraulic stimulation experiments in low permeability granitic rocks: Journal of Geophysical Research: Solid Earth, **86**, B9, 7855-7864.
Walter, W. R., and J. N. Brune, 1993, Spectra of seismic radiation from a tensile crack: Journal of Geophysical Research: Solid Earth, **98**, B3, 4449-4459.